Contributions to Mineralogy and Petrology (2018) 173:2
https://doi.org/10.1007/s00410-017-1427-0

ORIGINAL PAPER

Experimental determination of magnesia and silica solubilities in graphite-saturated and redox-buffered high-pressure COH fluids in equilibrium with forsterite + enstatite and magnesite + enstatite

Carla Tiraboschi[1] · Simone Tumiati[2] · Dimitri Sverjensky[3] · Thomas Pettke[4] · Peter Ulmer[5] · Stefano Poli[2]

Received: 21 May 2017 / Accepted: 20 November 2017 / Published online: 1 December 2017
© Springer-Verlag GmbH Germany, part of Springer Nature 2017

Abstract

We experimentally investigated the dissolution of forsterite, enstatite and magnesite in graphite-saturated COH fluids, synthesized using a rocking piston cylinder apparatus at pressures from 1.0 to 2.1 GPa and temperatures from 700 to 1200 °C. Synthetic forsterite, enstatite, and nearly pure natural magnesite were used as starting materials. Redox conditions were buffered by Ni–NiO–H_2O ($\Delta FMQ = -0.21$ to -1.01), employing a double-capsule setting. Fluids, binary H_2O–CO_2 mixtures at the *P, T*, and fO_2 conditions investigated, were generated from graphite, oxalic acid anhydrous ($H_2C_2O_4$) and water. Their dissolved solute loads were analyzed through an improved version of the cryogenic technique, which takes into account the complexities associated with the presence of CO_2-bearing fluids. The experimental data show that forsterite + enstatite solubility in H_2O–CO_2 fluids is higher compared to pure water, both in terms of dissolved silica ($mSiO_2 = 1.24$ mol/kg_{H2O} versus $mSiO_2 = 0.22$ mol/kg_{H2O} at $P = 1$ GPa, $T = 800$ °C) and magnesia ($mMgO = 1.08$ mol/kg_{H2O} versus $mMgO = 0.28$ mol/kg_{H2O}) probably due to the formation of organic C–Mg–Si complexes. Our experimental results show that at low temperature conditions, a graphite-saturated H_2O–CO_2 fluid interacting with a simplified model mantle composition, characterized by low MgO/SiO_2 ratios, would lead to the formation of significant amounts of enstatite if solute concentrations are equal, while at higher temperatures these fluid, characterized by MgO/SiO_2 ratios comparable with that of olivine, would be less effective in metasomatizing the surrounding rocks. However, the molality of COH fluids increases with pressure and temperature, and quintuplicates with respect to the carbon-free aqueous fluids. Therefore, the amount of fluid required to metasomatize the mantle decreases in the presence of carbon at high *P–T* conditions. COH fluids are thus effective carriers of C, Mg and Si in the mantle wedge up to the shallowest level of the upper mantle.

Keywords Mantle mineral solubility · COH fluids · Experimental petrology · Piston cylinder experiments · Cryogenic LA-ICP-MS

Introduction

High-pressure aqueous fluids are able to transport significant amounts of dissolved species derived from interaction with rock-forming minerals (Manning 1994). Experimental constraints on the extent of mineral dissolution are therefore

Communicated by Othmar Müntener.

Electronic supplementary material The online version of this article (https://doi.org/10.1007/s00410-017-1427-0) contains supplementary material, which is available to authorized users.

✉ Carla Tiraboschi
carla.tiraboschi@unimib.it

[1] Dipartimento di Scienze dell'Ambiente e della Terra, Università degli Studi di Milano Bicocca, piazza della Scienza 4, 20126 Milano, Italy

[2] Dipartimento di Scienze della Terra, Università degli Studi di Milano, via Mangiagalli 34, 20133 Milano, Italy

[3] Department of Earth & Planetary Sciences, Johns Hopkins University, 3400 N. Charles Street, Baltimore, MD 21218, USA

[4] Institut für Geologie, Universität Bern, Baltzerstrasse 1+3, 3012 Bern, Switzerland

[5] Institut für Geochemie und Petrologie, ETH Zürich, Clausiusstrasse 25, 8092 Zürich, Switzerland

crucial to understand metasomatic processes closely related to the mass transport of elements by high-pressure fluids. For example, quartz dissolution in H_2O at pressures and temperatures ranging from 0.1 to 2.0 GPa and 500 to 900 °C shows an increase of the total dissolved silica ($SiO_{2,aq}$) in H_2O with increasing P and T (Anderson and Burnham 1965; Manning 1994). The amount of solutes deriving from the dissolution of mantle minerals such as forsterite and enstatite in high-pressure fluids has been also extensively investigated in systems containing only pure water as volatile component (Nakamura and Kushiro 1974; Ryabchikov et al. 1982; Manning and Boettcher 1994; Zhang and Frantz 2000; Newton and Manning 2002). Experimental evidence indicated that lower amounts of dissolved silica result from the dissolution of Mg-silicates (forsterite and enstatite) in aqueous fluids compared to the dissolution of quartz. In the system SiO_2–H_2O–CO_2, mixed fluids show decreasing amounts of $SiO_{2,aq}$ with increasing content of CO_2 in the fluid (e.g., Newton and Manning 2000). However, the effect of CO_2 addition to aqueous fluids in equilibrium with mantle minerals has remained experimentally unexplored, although carbon dioxide is thought to be a significant volatile species in subduction-related fluids occurring at the slab–mantle interface (e.g., Tumiati et al. 2017).

Forsterite and enstatite solubility in H_2O

In early studies of silicate solubilities in aqueous fluids in the MgO–SiO_2–H_2O (MSH) system at deep crustal and upper mantle conditions ($P < 2$ GPa and $T < 1300$ °C), the composition of the fluid phase has been estimated from phase relations projected to the SiO_2–H_2O subsystem, assuming that the amount of MgO in the fluid was negligible at the investigated condition (Nakamura and Kushiro 1974; Ryabchikov et al. 1982; Zhang and Frantz 2000). At 1.5 GPa and temperatures from 1280 to 1340 °C, aqueous fluids saturated with forsterite and enstatite are able to dissolve significant amounts of SiO_2 ranging from 18 wt% at 1280 °C to 22 wt% at 1310 °C (Nakamura and Kushiro 1974). At 3 GPa and 1000 °C, the MgO/SiO_2 ratio increases with pressure and reaches unity at 3 GPa and 1000 °C in a fluid containing > 30 wt% dissolved silica (Ryabchikov et al. 1982).

Another approach to quantify the amount of solutes was to extract both fluids and precipitates from piston–cylinder experiments (Manning and Boettcher 1994) and analyzing them by means of inductively coupled plasma mass spectrometry (ICP-MS). Experimental data showed that at $P = 1$ GPa and $T = 700$ °C, the concentration of MgO in the solution was below the detection limit (< 0.005 mol/kg_{H2O}), while the dissolved SiO_2 in H_2O was 0.1 mol/kg_{H2O}.

With a third approach, the weight loss technique (Newton and Manning 2002), solubilities of forsterite + enstatite were measured from 0.4 to 1.5 GPa and $T = 700$–900 °C. Silica concentrations at 1 GPa increase from 0.16 mol/kg_{H2O} at 700 °C to 0.50 mol/kg_{H2O} at 900 °C, showing a small increase with pressure between 0.7 and 1.4 GPa. The higher solubility data compared to those retrieved by Zhang and Frantz (2000) (0.34 mol/kg_{H2O} at 1 GPa and 900 °C) were attributed by Newton and Manning (2002) to the quenching method employed by the authors. It was suggested that decreasing temperature at nearly constant pressure could lead to the formation of hydrothermal enstatite, as the P, T path during quenching passed through the stability field of enstatite. The presence of enstatite having formed upon quench could have caused a misinterpretation of phase equilibrium boundaries by Zhang and Frantz (2000), leading to slight underestimation of the silica content of the fluid.

Synchrotron X-ray fluorescence spectroscopy (S-XRF), coupled with an externally heated diamond anvil cell (DAC), was employed to investigate enstatite and forsterite solubility in aqueous fluids from 0.5 to 5.8 GPa and 800–1000 °C (Kawamoto et al. 2004a). At 3 GPa and 1000 °C, it was observed that the MgO/SiO_2 ratio changes from SiO_2-rich to MgO-rich fluid, probably due to structural changes in liquid water (Kawamoto et al. 2004b).

At higher pressure conditions, the diamond trap technique (Ryabchikov et al. 1989; Baker and Stolper 1994) has been employed to trap precipitates and melt in a diamond-powder layer placed in the experimental capsule and subsequently analyzed via laser ablation ICP-MS (LA-ICP-MS). Employing this technique, the MSH system was investigated from 6 to 10.5 GPa and temperatures from 900 to 1200 °C (Stalder et al. 2001) and the second critical end point was located above 11 GPa (Melekhova et al. 2007) employing an improved version of the diamond trap technique, where the diamond layer is kept frozen during the LA-ICP-MS analyses (freezing technique; Kessel et al. 2004, 2005a, 2005b).

Carbonate solubility in H_2O

Carbonate dissolution in H_2O has been investigated experimentally by several authors (Walther and Long 1986; Fein and Walther 1989; Caciagli and Manning 2003; Sanchez-Valle et al. 2003). The weight loss technique (Manning 1994) was employed to investigate the dissolution of calcite in pure water up to $P = 1.6$ GPa and $T = 500$–900 °C (Caciagli and Manning 2003), extending the pressure range of previous calcite solubility studies (e.g., Fein and Walther 1989). Results indicate that the solubility of calcite at 1 GPa increases with increasing temperature from 0.016 mol/kg_{H2O} at 500 °C to 0.057 mol/kg_{H2O} to 750 °C. At pressure up to 3.6 GPa and low temperature conditions ($T = 250$ °C), strontianite dissolution in H_2O was retrieved employing an externally heated DAC and synchrotron X-ray fluorescence spectroscopy (Sanchez-Valle et al. 2003).

A significant effort has been made to develop thermodynamic models to predict carbonate behavior in aqueous fluids (Dolejs and Manning 2010; Pan et al. 2013; Facq et al. 2014; Pan and Galli 2016). Results indicate that HCO_3^- is the dominant species in aqueous fluids dissolving aragonite below 4 GPa and low temperature conditions (300–400 °C), while at higher pressures CO_3^{2-} becomes the dominant species, in contrast to the previously hypothesized predominance of $CO_{2,aq}$ in aqueous fluids (Facq et al. 2014). Moreover, according to theoretical calculations, magnesite, insoluble in water at ambient condition, becomes soluble at 10 GPa (Pan et al. 2013).

Solubilities in mixed H_2O–CO_2 fluids

Experimental data on mineral dissolution in mixed H_2O–CO_2 fluid are available only for quartz (Walther and Orville 1983; Newton and Manning 2000, 2009; Shmulovich et al. 2006), albite and diopside (Shmulovich et al. 2001), and suggests that the presence of CO_2 lowers the solute content in the fluid by decreasing the water activity (i.e., by increasing the CO_2 content).

To analyze the solubility of quartz in H_2O–CO_2 mixed fluids, Walther and Orville (1983) developed an extraction quench-hydrothermal apparatus. In these experiments, performed in cold seal vessels, the pressure was limited to 0.2 GPa at $T < 600$ °C. Results showed a decrease in quartz solubility with increasing amounts of CO_2 in the fluid.

Another option is to extract and collect the solutes from piston cylinder experiments (Schneider and Eggler 1986). Solutes were mixed with $LiBO_2$ and fused in graphite capsule at $T = 1000$ °C for 10 min. Glasses were then analyzed using an electron microprobe. The solubility of different types of peridotites (amphibole-, phlogopite-, and clinopyroxene-bearing peridotite) and single minerals in mixed H_2O–CO_2 fluids were retrieved at $P = 1.5$–2 GPa and $T = 600$–1100 °C. Results showed that the addition of CO_2 (9 mol%) to the aqueous fluid strongly depressed the solubility of silicates by approximately one order of magnitude.

A modified version of the weight loss technique was employed to determine the activity–composition relations in CO_2–H_2O solutions (Aranovich and Newton 1999). The capsule was frozen in liquid nitrogen and punctured with a needle while still frozen. The immediate weight loss was ascribed to CO_2 escape. The capsules were then dried and reweighed to retrieve the H_2O content. This technique, applied on double-capsules, was also used to investigate quartz dissolution in H_2O–CO_2 at $P = 0.2$–1.5 GPa and $T = 500$–900 °C (Newton and Manning 2000, 2009). The solubility of SiO_2 in the fluid decreases strongly with increasing CO_2, in agreement with previous experimental data.

Experimental

Starting materials

Carbon-saturated H_2O–CO_2 fluids were generated starting from oxalic acid anhydrous (OAA; $H_2C_2O_4$), water and glassy carbon spherical powder (grain size 80–200 µm). The thermal dissociation of OAA generates a CO_2–H_2 fluid according to the reaction:

$$H_2C_2O_4 = 2CO_2 + H_2. \quad (1)$$

A known amount of water, added to the capsule through a microsyringe, allowed to obtain a roughly equimolar CO_2–H_2O starting fluid phase with XCO_2 [$= CO_2/(H_2O + CO_2)$] = 0.5. As an internal standard for LA-ICP-MS data quantification (see Kessel et al. 2004), water was doped with 590 µg/g of cesium [$Cs(OH)_2$].

Two different starting materials were considered: (1) a mixture of forsterite and minor enstatite (FoEn) and (2) a mixture of enstatite, magnesite and minor forsterite (EnMgs). Forsterite and enstatite were synthesized from dried nanocrystalline $Mg(OH)_2$ (Sigma-Aldrich, 99.9% purity) and silicon dioxide (Balzers, 99.9% purity), mixed in stoichiometric proportions, pelletized and loaded in a vertical furnace at 1500 °C for 24 h. Synthesis products were ground in ethanol for 1 h, dried and characterized by X-ray powder diffraction analysis (Bruker, AXS D8 Advance, ETH Zurich; Philips X'pert MPD, University of Milan). Natural magnesite from Pinerolo (Italy), checked for purity through electron microscopy and microprobe analyses (Jeol 8200 Superprobe, University of Milan), was ground under ethanol for 1 h and dried. The resulting composition of the mixtures, derived by Rietveld analysis, are: (1) forsterite 83.2 wt%, enstatite 16.7 wt%, and cristobalite 0.1 wt% for the starting material identified as FoEn, and (2) magnesite 44.2 wt%, enstatite 39 wt%, forsterite 15.3 wt%, and cristobalite 1.5 wt% for the starting material EnMgs.

To collect fluids and solutes, a layer of diamond crystals with grain size of 20 µm was placed between two layers of the starting mineral assemblages (FoEn or EnMgs). All experimental runs were performed at fluid-saturated conditions, with total fluids accounting for ~ 20 wt%. An additional experimental run was performed at $P = 1$ GPa and $T = 800$ °C employing the starting material FoEn and a single Au capsule to measure the solubility of the assemblage forsterite + enstatite in pure water for comparison with previously published results (Newton and Manning 2002).

Experimental strategy

As the volatile composition of a graphite-saturated COH fluid is dependent on the redox state of the system, all the experimental runs were performed employing the double-capsule technique (Eugster and Skippen 1967) and the nickel–nickel oxide (NNO) buffer to constrain the redox conditions.

The inner $Au_{50}Pd_{50}$ capsule was loaded with the starting materials, FoEn or EnMgs, OAA, Cs-doped water, graphite and diamonds (Fig. 1). The outer capsule (Au at $T < 1000$ °C, Pt at $T > 1000$ °C) contained the inner capsule, NNO and H_2O. The NNO buffer fixes the chemical potential of H_2 (fH_2^{NNO}) in the H_2O-only fluid of the outer capsule. As long as the phases Ni, NiO and H_2O are present, the fugacity of H_2 is fixed by the reaction:

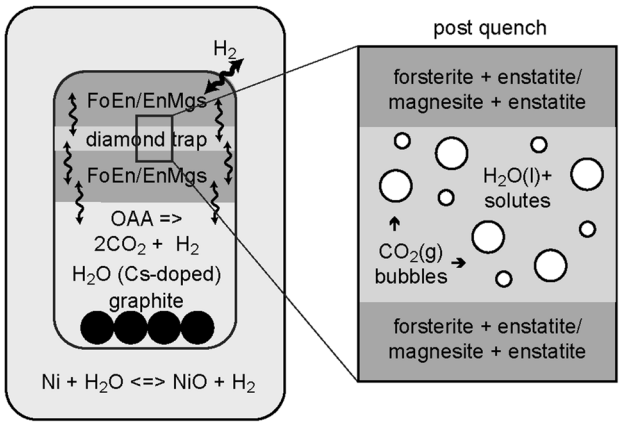

Fig. 1 Experimental strategy adopted to investigate the solubilities of forsterite + enstatite and magnesite + enstatite in the MS + COH system. The double-capsule technique is employed to constrain the fH_2 conditions (and consequently the fO_2) by the assemblage Ni + NiO + H_2O (NNO buffer)

$$Ni + H_2O = NiO + H_2. \quad (2)$$

The $Au_{50}Pd_{50}$ alloy of the inner capsule is permeable to hydrogen; therefore, the chemical potential of H_2 is expected to be homogeneous in the inner and the outer capsules. Since the inner capsule will contain in general a fluid with other COH species (such as CO_2) in addition to H_2O, the oxygen chemical potential in the inner capsule will be lower (Luth 1989) and can be calculated by thermodynamic modeling along with the volatile composition of the graphite-saturated COH fluid. In all experimental runs, the NNO buffer assemblage was preserved after the quench. Graphite was preserved at pressure ≤ 2 GPa and temperatures below 1200 °C.

The fugacities of oxygen (fO_2^{NNO}) and hydrogen (fH_2^{NNO}) fixed in the outer capsule by NNO were calculated employing the software package Perple_X (Connolly 1990; http://www.perplex.ethz.ch/) and the thermodynamic dataset of Holland and Powell (1998). The routines "vertex" and "fluids" were used first to calculate the fugacity of hydrogen fixed in the outer capsule by NNO + H_2O (Perple_X equation of state no. 16; H–O HSMRK/MRK hybrid EoS). Then, we calculated the speciation of the COH fluid through the Excel spreadsheet GFluid (Zhang and Duan 2010) with the EoS of Zhang and Duan (2009) and a modified H_2 fugacity coefficient (γH_2) changing dynamically as a function of X(O), fitted from the EoS of Connolly and Cesare (1993). This model has been proved to reproduce the composition of COH fluids in the pure C–O–H system (Tumiati et al. 2017). By assuming that fH_2 of the COH fluid in the inner capsule is equal to fH_2^{NNO}, we were able to calculate the molar fractions of volatiles (H_2O, CO_2, CO, CH_4, H_2 and O_2) at the investigated pressure and temperature conditions. The predicted fluids are mainly composed of H_2O and CO_2, with XCO_2 ratios changing as a function of pressure and temperature (Table 1).

Table 1 Modeled volatile compositions with log fO_2 and log fH_2 values of graphite-saturated COH fluids buffered externally for fH_2 with the double-capsule technique, at selected conditions of pressure and temperature

Run	17	29	7	6	5	10	8	9	20
P (GPa)	1	1	1	1	1	1.5	1.5	1.5	2
T (°C)	700	800	900	1000	1100	800	900	1000	1100
log fO_2 outer capsule	−15.8	−13.5	−11.6	−9.9	−8.6	−13.2	−11.4	−9.8	−8.2
log fH_2 outer capsule = inner capsule	1.64	1.78	1.88	1.97	2.04	2.14	2.24	2.38	2.67
Modeled composition at fixed fH_2 (mol%)									
H_2O	37.7	28.8	22.2	17.3	13.6	40.0	32.3	25.9	31.0
CO_2	62.0	70.4	75.9	78.7	79.0	59.6	66.8	72.0	66.7
CO	0.21	0.66	1.71	3.74	7.18	0.31	0.83	1.90	2.14
H_2	0.04	0.08	0.12	0.18	025	0.04	0.08	0.12	0.14
CH_4	0.05	0.06	0.06	0.06	0.06	0.05	0.05	0.06	0.07
XCO_2	0.62	0.71	0.77	0.81	0.85	0.60	0.67	0.74	0.68
log fO_2 inner capsule	−16.2	−14.3	−12.7	−11.4	−10.2	−13.6	−12.0	−10.7	−9.1

Pertinent experimental runs are shown with red labels in Fig. 2. EoS by Zhang and Duan (2009) with dynamic H_2 fugacity coefficient by Connolly and Cesare (1993)

At $T > 700$ °C, the COH volatile composition is enriched in CO_2 compared to the starting equimolar H_2O–CO_2 composition given by OAA and H_2O. Equilibration of the COH fluid is accomplished by these coupled reactions:

$$H_2O \rightleftarrows H_2 + {}^1/_2O_2, \quad (3)$$

$$C + 2O \rightleftarrows CO_2, \quad (4)$$

which can be condensed to the following water- (and graphite-) consuming reaction:

$$C + 2H_2O \rightleftarrows CO_2 + 2H_2. \quad (5)$$

The equilibration of the COH fluid at the experimental conditions implies that CO_2 is produced in the inner capsule by oxidation of graphite, a process that requires oxygen, which is taken from the dissociation of water. As a consequence, not only the XH_2O [$= H_2O/(H_2O + CO_2)$] of the COH fluid, but also the absolute quantity of water decreases in the inner capsule until equilibrium is reached at the experimental P and T conditions.

A P–T pseudosection for the system MS + COH at fO_2^{NNO} conditions was compiled employing the software Perple_X (Connolly 1990). As the composition of the COH fluid is constrained by the oxygen fugacity conditions, variable in the P–T field, the fO_2^{NNO} conditions retrieved by thermodynamic modeling were fitted in equation:

$$\ln fO_2 = 10.75 + (-50077 + 0.32196P)/T, \quad (6)$$

(P in bar and T in K), and the COH volatile composition in the P–T field is calculated accordingly. By fixing fO_2^{NNO}, the two resulting univariants (black solid lines in Fig. 2) are given by the reactions:

$$\text{Forsterite} + \text{COH fluid}\left(fO_2^{NNO}\right) = \text{Enstatite} + \text{Magnesite}, \quad (7)$$

and

$$\text{Enstatite} + \text{COH fluid}\left(fO_2^{NNO}\right) = \text{Talc} + \text{Magnesite}. \quad (8)$$

On the basis of the predicted stable assemblage in the P–T field, we select as starting materials either FoEn or EnMgs (see Supplementary Material).

Experimental conditions

Experiments were carried out in a rocking piston-cylinder apparatus at pressures from 1.0 to 2.1 GPa and temperatures from 700 to 1200 °C. The rocking piston–cylinder apparatus was employed to guarantee the homogeneity of the sample through a rotation of 180°. The rotation induces Rayleigh-Taylor instabilities, forcing the fluid to migrate and promoting chemical homogenization (Schmidt and Ulmer 2004). During the heating stage, the piston–cylinder rotated continuously (one turn of 180° every 30 s), and then the rotation

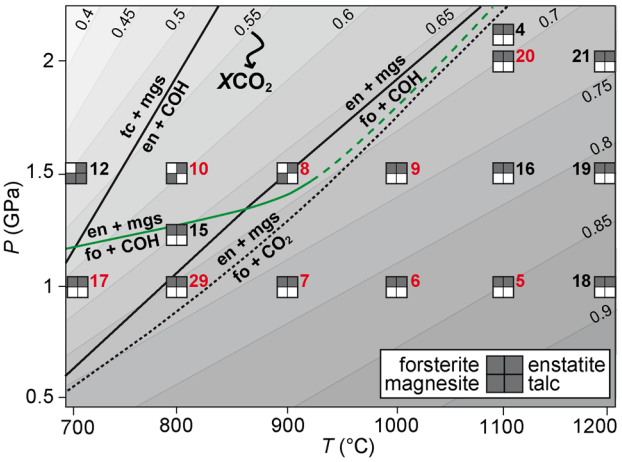

Fig. 2 Phase assemblages in the MS + COH system buffered at fH_2^{NNO} conditions as a function of pressure and temperature. Run numbers are reported next to the phase assemblages. The experimental runs in which we were able to retrieve the solute content are shown with red labels. The labels on gray-shaded contours represent XCO_2 values determined through thermodynamic modeling. Reactions in black solid lines are reported for reference and were calculated by means of thermodynamic modeling (talc: tc; forsterite: fo; enstatite: en; magnesite: mgs; COH: COH fluid). Solid green line represents the reaction forsterite + COH fluid = enstatite + magnesite drawn on the basis of the mineral assemblages observed in textural equilibrium. The experimentally determined reaction forsterite + CO_2 = enstatite + magnesite from Koziol and Newton (1998) is reported for reference as black dotted line

interval was changed to 100 s. Experiments were performed for an average run time of 48 h. Quench rates are variable from 25 to 40 °C/s. The assembly consists in NaCl, Pyrex, a graphite heater and graphite disks at the bottom. The capsule was embedded in MgO rods filled with MgO powder. After the experimental run, the recovered capsules were cleaned with diamond router bites and rinsed in a diluted HCl solution for 5 h to eliminate residues of MgO from the capsule.

Analytical technique

The solute content in the fluid was measured through the cryogenic laser ablation ICP-MS technique (Aerts et al. 2010), a modified version of the freezing technique (Kessel et al. 2004), which was applied in this experimental study for the first time on double-capsules bearing COH fluids. The recovered experimental capsule was mounted on a freezing stage representing the base of the laser ablation cell, consisting of a stack of two Peltier elements, surrounded by plastic to thermally insulate the elements from the atmosphere (Aerts et al. 2010). The capsule holder is inserted into a copper block in direct contact with the Peltier elements and cooled to $T = -35$ °C. Conventionally, frozen single capsules can be cut open by hand using a razor blade (Kessel

et al. 2004; Aerts et al. 2010). However, this method was hardly possible (and thus poorly controlled) in the present case because of the toughness of double-capsules. Consequently, capsule cutting was performed using a mechanical cutting device onto the freezing stage (Fig. 3a). This device allows to expose a longitudinal cross section of the capsule by fastening a screw that pushes a cutter blade mechanically guided through a copper vice holding the capsule (Fig. 3b), while temperature is kept at − 35 °C in a box flushed with dry Ar. Once the capsule is opened, the device is removed from the freezing stage together with the upper part of the capsule holder. The upper half of the capsule is inspected with a binocular microscope to help locate the diamond trap, while the lower part, always kept frozen, is covered by the ablation cell top (Fig. 3c) and transferred to the microscope stage for LA-ICP-MS measurements.

The analyses were performed using a 193 nm ArF GeoLas Pro excimer laser system coupled to an ELAN DRC-e quadrupole mass spectrometer at the University of Bern. We analyzed the diamond trap for ^{24}Mg, ^{25}Mg, ^{26}Mg, ^{29}Si, ^{62}Ni, ^{133}Cs, ^{195}Pt and ^{197}Au, using a 60 µm beam diameter, ~ 13 J/cm^2 laser fluence and 5 Hz repetition rate. For Mg, all three isotopes were recorded to constrain the effect of polyatomic gas interferences (^{12}C^{12}C, ^{12}C^{13}C, ^{12}C^{14}N) on the final results. At − 35 °C set in the freezing stage, the CO_2 fraction unmixed from the COH fluid upon quench is not frozen, thus accounting for the low coherence of the trap during laser ablation measurement (and resulting craters were not well defined). Data were acquired in blocks of up to ~ 10 individual sample analyses bracketed by three analysis of the standard NIST SRM610, placed in the ablation chamber with the sample. Background was taken for ~ 50 s and the sample signal, on the diamond trap or on the solid residue, was collected for ~ 20 s. LA-ICP-MS data reduction was performed employing the software Sills (Guillong et al. 2008; http://www.geopetro.ethz.ch/research/orefluids/software) and in-house spreadsheets to calculate solute concentrations employing rigorous limits of detection filtering (Pettke et al. 2012) for each element and each measurement individually.

The cryogenic LA-ICP-MS technique was originally developed to analyze the solute content in systems containing only H_2O as volatile component. Cesium, introduced in the starting material, was employed as internal standard for data quantification, because it is a highly incompatible element that partitions completely into the fluid with the given mineral assemblages. In our experiments, we introduced a known amount of water doped with 590 µg/g Cs [as $Cs(OH)_2$]. As the initial Cs/H_2O ratio is fixed, once the Cs concentration in the fluid phase coexisting with minerals at run *P* and *T* is known, solute concentrations of the fluid can be calculated (Kessel et al. 2004). However, compared to experiments bearing aqueous fluids coexisting with anhydrous silicates, our double-capsule, COH-bearing experiments are more complex, because (1) there is one fluid phase at run conditions (mostly a $H_2O + CO_2$ mixed fluid, plus solutes), exsolving two fluid phases (liquid H_2O + solutes, and gaseous CO_2) at quench conditions (see Fig. 1) and (2) the initial Cs/H_2O is not fixed in our experiments, because the water content in the runs is variable, depending on *P, T* and fO_2 conditions. In double-capsule arrangements, H_2 is in fact a mobile component that can be added or removed from the system through diffusion in and out the inner capsule. These conditions imply that the LA-ICP-MS data on systems bearing COH fluids refer to the aqueous part of fluids only, assuming that no solutes escape with the carbonic gas species upon capsule opening. Moreover, the latter point implies the initial Cs concentration cannot be used as an internal standard, unless this value is corrected to the XH_2O in the fluid at run *P* and *T* conditions. To retrieve the amount of solutes in terms of

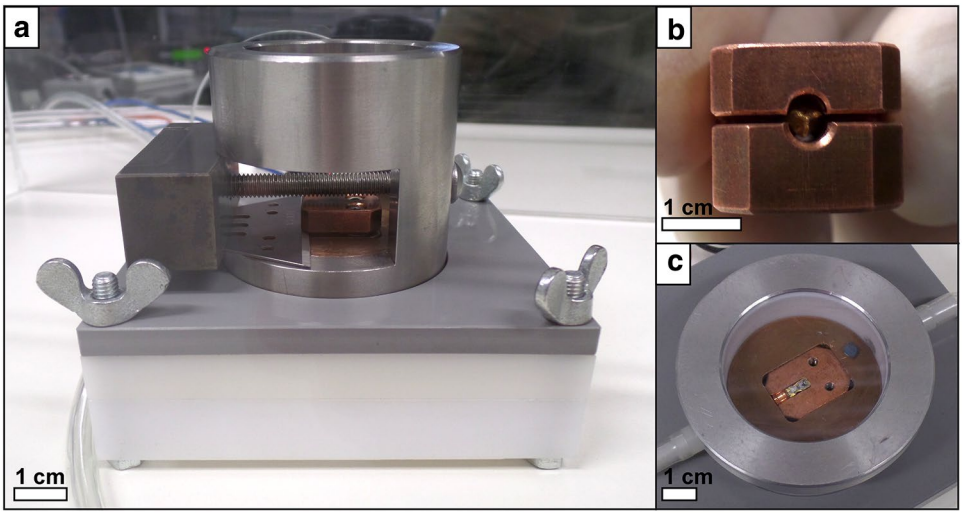

Fig. 3 **a** The freezing stage equipment employed to open the tough double-capsule and to perform LA-ICP-MS measurements of the frozen diamond trap; **b** the copper capsule holder; **c** the freezing stage laser ablation cell hosting the capsule and the external standard material (blue chip) ready for the laser ablation analysis

mol/kg_{H2O}, a correction for the change in total water mass present in the inner capsule relative to the initial water mass loaded into the capsule is thus required.

If H_2O is consumed during fluid re-equilibration at run conditions, Cs concentration in the residual water increases; if H_2O is produced, Cs concentration decreases. We estimated the corrected Cs concentration at run P and T using a model, which assumes that fluid equilibration at NNO hydrogen fugacity conditions is governed only by H_2 mobility and no hydration or carbonation reactions involving minerals occur in the capsule charge. As long as these two assumptions are valid, it is possible to estimate the amount of Cs in the inner capsule using the following dilution equation:

$$C_i\mathrm{Cs} \times n_i\mathrm{H_2O} = C_f\mathrm{Cs} \times n_f\mathrm{H_2O}, \quad (9)$$

where C_iCs is the initial concentration of Cs in the aqueous solution loaded into the capsule (590 µg/g) and C_fCs is the final concentration of Cs after fluid equilibration at $f\mathrm{H_2}^{\mathrm{NNO}}$ conditions. $n_i\mathrm{H_2O}$ and $n_f\mathrm{H_2O}$ are the initial and final number of H_2O moles.

The final Cs concentration will be given by:

$$C_f\mathrm{Cs} = \frac{C_i\mathrm{Cs} \times n_i\mathrm{H_2O}}{n_f\mathrm{H_2O}}. \quad (10)$$

As $n_i\mathrm{H_2O}$ is known, i.e., the initial amount of water charged into the capsule, Eq. (10), can be solved as long as $n_f\mathrm{H_2O}$ is constrained. Solute concentrations in the pure water fraction of the fluid at run P and T can thus be calculated. For one experimental run, performed at 1 GPa and 800 °C, the volatile speciation of the fluid was retrieved experimentally by employing the capsule-piercing QMS technique (Tiraboschi et al. 2016) instead of calculating the amount of H_2O and CO_2 through thermodynamic modeling. The volatile composition consists of CO_2 (84.2 wt%) and H_2O (15.8 wt%). Compared to the experimental model employed to quantify the internal standard, the experimental volatile speciation appears to be enriched in CO_2 (see Table 1). The discussion relative to the different volatile speciation is presented elsewhere (Tumiati et al. 2017). However, since the experimental result shows that the amount of H_2O in the inner capsule could be more variable than expected, the solubility of silica and magnesia were also calculated by varying the amount of H_2O in the experiments (plus or minus 50%; available as Supplementary Material). Varying the amount of water does not affect significantly the amount of solutes, the variations of which are dominated by the analytical error. Consequently, the volatile speciation derived from thermodynamic modeling was employed to retrieve the solubility for all the other experimental runs.

For the experimental runs performed in the stability field of magnesite, we employed the EnMgs starting material to minimize the amount of newly formed carbonates. X-ray maps of elements and principal component analysis (PCA) were used to evaluate the relative abundances of solid phases in the experimental runs and estimate the amount of CO_2 consumed to form new magnesite crystals. In fact, the initial amount of water charged in the capsule ($n_i\mathrm{H_2O}$) will readjust if part of the initial CO_2 is consumed to form carbonates, as the system is buffered at NNO hydrogen fugacity conditions. To maintain the CO_2/H_2O ratio determined by the hydrogen fugacity conditions, the amount of H_2O has to decrease in the inner capsule. Consequently, the experimental runs performed in the magnesite stability field required an additional Cs correction. Capsules were inspected at the electron microscope (JEOL 8200 Superprobe, University of Milan) for presence of quench precipitate magnesite in the diamond layer. Then the capsules were embedded in epoxy and polished, to perform wavelength-dispersive X-ray spectroscopy (WDS) analyses and X-ray elemental maps of elements.

Results

In Fig. 2, the run products are displayed together with the experimental carbonation curve of forsterite, determined on the basis of textural observations. The $X\mathrm{CO_2}$ of the fluid is shown as gray shaded contours. At the P–T–$f\mathrm{O_2}$ conditions investigated, we observed three mineral assemblages: (1) forsterite + enstatite (fo + en); (2) talc + magnesite (tc + mgs); (3) enstatite + magnesite (en + mgs). The majority of the experimental runs that started with the FoEn mix gave the same run product of forsterite + enstatite after the quench, with the exception of two experimental runs: (1) 1.5 GPa and 900 °C and (2) 2 GPa and 1200 °C. At 1.5 GPa and 900 °C, we observed newly formed magnesite from the forsterite + enstatite assemblage (Fig. 4a). At 2 GPa and 1200 °C, the experimental run presents a sponge-like texture consisting of silica precipitates (Fig. 4b) with small dispersed enstatite crystals. No forsterite crystals were identified at these conditions; however, it has to be noted that the capsule was severely damaged during the cutting procedure for LA analyses. At 1.5 GPa and 800 °C, the experimental run performed employing the EnMgs starting material lead to the assemblage enstatite + magnesite, with no residual forsterite observed. At 1.5 GPa and 700 °C, the EnMgs starting material yielded to the assemblage enstatite + talc + residual magnesite, and at 1.2 GPa and 800 °C forsterite coronas were observed surrounding magnesite crystals (Fig. 4c).

The solubility results expressed as mol/kg_{H2O} are reported in Table 2, together with the total amounts of solute in wt% and the calculated Cs concentrations (in µg/g) prevailing at run conditions in the pure water. No solubility data were obtained above 2 GPa and 1100 °C and at 1.5 GPa and 1100 °C, as the diamond trap was not completely preserved

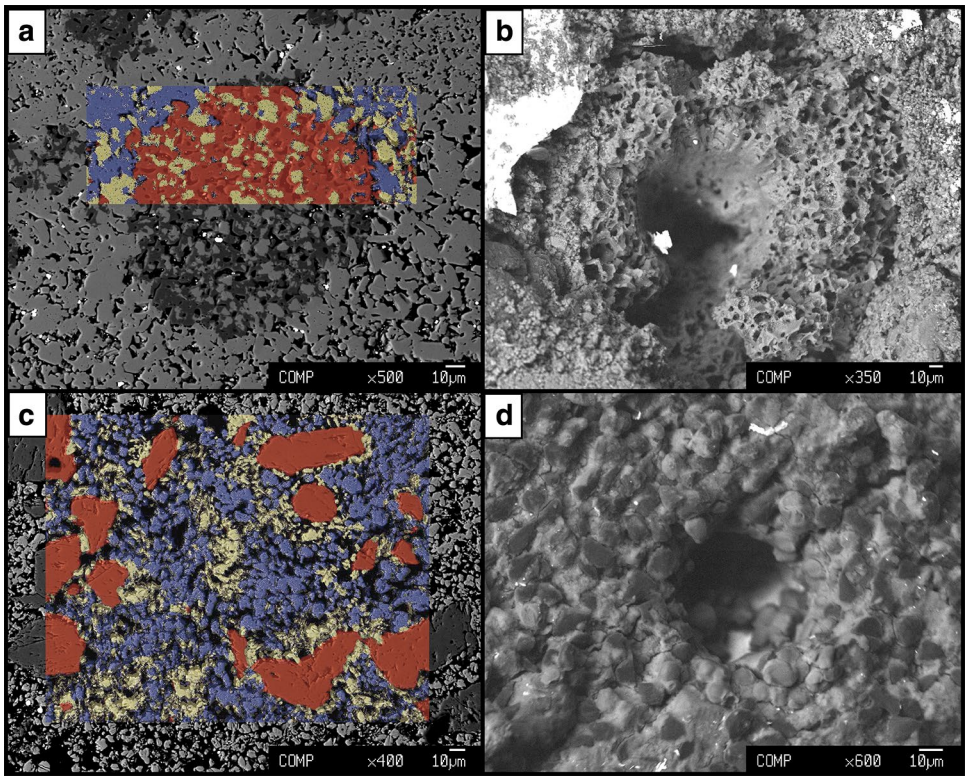

Fig. 4 Backscattered electron images of representative runs. **a** Magnesite formation at 1.5 GPa and 900 °C. Principal component analysis is superposed to emphasize phase distribution (magnesite in red, enstatite in blue, forsterite in yellow); **b** silica precipitates at 2 GPa and 1200 °C; **c** forsterite coronas around magnesite at 1.2 GPa and 800 °C. Principal component analysis is superposed (magnesite in red, enstatite in blue, forsterite in yellow); **d** diamonds dispersed at $P = 1.5$ GPa and $T = 1200$ °C

Table 2 Solubility of forsterite + enstatite and magnesite + enstatite in experimental fluids at fH_2^{NNO}, measured by laser ablation ICP-MS using the cryogenic technique and expressed as moles of SiO_2 and MgO per kilogram of water (mol/kg_{H2O}) and as weight percentage in the water fraction of the fluid (wt%)

Run	P (GPa)	T (°C)	n	$mSiO_2$ (mol/kg_{H2O})	$mMgO$ (mol/kg_{H2O})	Total solutes (wt%)	Cs (µg/g)	XCO_2
Forsterite + Enstatite + COH fluid								
17	1	700	3	0.85 (0.15)	0.67 (0.06)	7.2	830	0.62
29	1	800	2	1.24 (0.19)	1.08 (0.10)	11	2140	0.84
7	1	900	3	2.56 (0.68)	1.38 (0.53)	17	1340	0.77
6	1	1000	1	3.87 (–)	3.51 (–)	27	1800	0.81
5	1	1100	1	4.21 (–)	6.90 (–)	35	2270	0.85
9	1.5	1000	1	4.32 (–)	6.51 (–)	34	1200	0.74
20	2	1100	2	4.60 (0.37)	6.12 (0.99)	34	1110	0.78
Magnesite + Enstatite + COH fluid								
10	1.5	800	2	0.41 (0.02)	0.47 (0.09)	4.2	1130	0.60
8	1.5	900	2	0.53 (0.23)	0.73 (0.29)	5.8	1440	0.67
Forsterite + Enstatite + H_2O								
22	1	800	3	0.22 (0.06)	0.28 (0.04)	2.4	590	–

Uncertainties are given in parentheses as 1 standard deviation of n analyses of the diamond trap. The concentration of the internal Cs standard in the water fraction, corrected taking into account the XCO_2 of the COH fluid, is also provided

at these conditions (Fig. 4b, d). Moreover, solubilities were not retrieved at 1.5 GPa and 700 °C and 1.2 GPa and 800 °C due to the lack of equilibrium between solid phases (i.e., magnesite in the talc + enstatite assemblage and forsterite coronas on magnesite relics).

Concerning analytical errors, Kessel et al. (2004) determined an uncertainty in the amount of H_2O in the fluid, derived from Cs analysis, ranging from 0.7 to 2.5%, which was more similar (or smaller) than the standard deviation of their data. In our case, for each experiment, we reported the standard deviation, as our values are higher compared to the

maximum uncertainty (2.5%) determined by Kessel et al. (2004). However, if only one laser ablation shot is available (experimental runs 6, 5 and 9), we consider a minimum analytical error corresponding to that given by Kessel et al. (2004).

Forsterite + enstatite assemblage

The SiO_2 contents reported as weight percentage in the water fraction of the fluid equilibrated with forsterite and enstatite (Table 2) increases with temperature from 0.85 ± 0.15 mol/kg_{H2O} at 1 GPa and 700 °C to 4.21 ± 0.04 mol/kg_{H2O} at 1 GPa and 1100 °C. The amount of SiO_2 tends to increase with pressure, reaching 4.60 ± 0.37 mol/kg_{H2O} at 2 GPa and 1100 °C (Fig. 5a). The MgO content also rises with T, from 0.67 ± 0.06 mol/kg_{H2O} at 1 GPa and 700 °C to 6.90 ± 0.07 mol/kg_{H2O} at 1 GPa and 1100 °C, while from 1 to 2 GPa at 1100 °C we observe identical mMgO values within errors (6.90 ± 0.04 mol/kg_{H2O} at 1 GPa; 6.12 ± 0.99 mol/kg_{H2O} at 2 GPa) (Fig. 5b).

The solubility of forsterite + enstatite in COH fluids was compared with the solubility of the same assemblage in pure water, by performing a dissolution experiment at $P = 1$ GPa and $T = 800$ °C (white dots in Fig. 5). At these conditions, SiO_2 dissolved in pure water (0.22 ± 0.06 mol/kg_{H2O}) is much lower than SiO_2 dissolved in the COH fluid (1.24 ± 0.19 mol/kg_{H2O}) (Fig. 5a). In a similar way also the MgO content from forsterite and enstatite dissolution in the COH fluid is higher compared to dissolution in H_2O: from 0.28 ± 0.04 mol/kg_{H2O} in H_2O to 1.08 ± 0.10 mol/kg_{H2O} in the MS + COH system (Fig. 5b).

Enstatite + magnesite assemblage

Two experimental runs were performed in the enstatite + magnesite stability field, above the forsterite carbonation reaction (see Fig. 2). For these experiments, the amount of SiO_2 and MgO in the aqueous fraction of the COH fluid was retrieved considering that a part of the initial CO_2 in the inner capsule was consumed to produce carbonate. The amount of SiO_2 at 1.5 GPa from 800 to 900 °C (Table 2) is similar within analytical error (0.41 ± 0.02 mol/kg_{H2O} at 800 °C; 0.53 ± 0.23 mol/kg_{H2O} at 900 °C; Fig. 5a), while the mMgO tends to increase with temperature from 0.47 ± 0.09 mol/kg_{H2O} at 800 °C to 0.73 ± 0.29 mol/kg_{H2O} (within the stated uncertainties; Fig. 5b). Compared to the forsterite + enstatite assemblage, the SiO_2 concentration in the fluid coexisting with enstatite + magnesite is significantly lower, suggesting a lower solubility of enstatite in the COH fluid compared to forsterite. The MgO content is lower compared to the fluid in equilibrium with forsterite and enstatite;

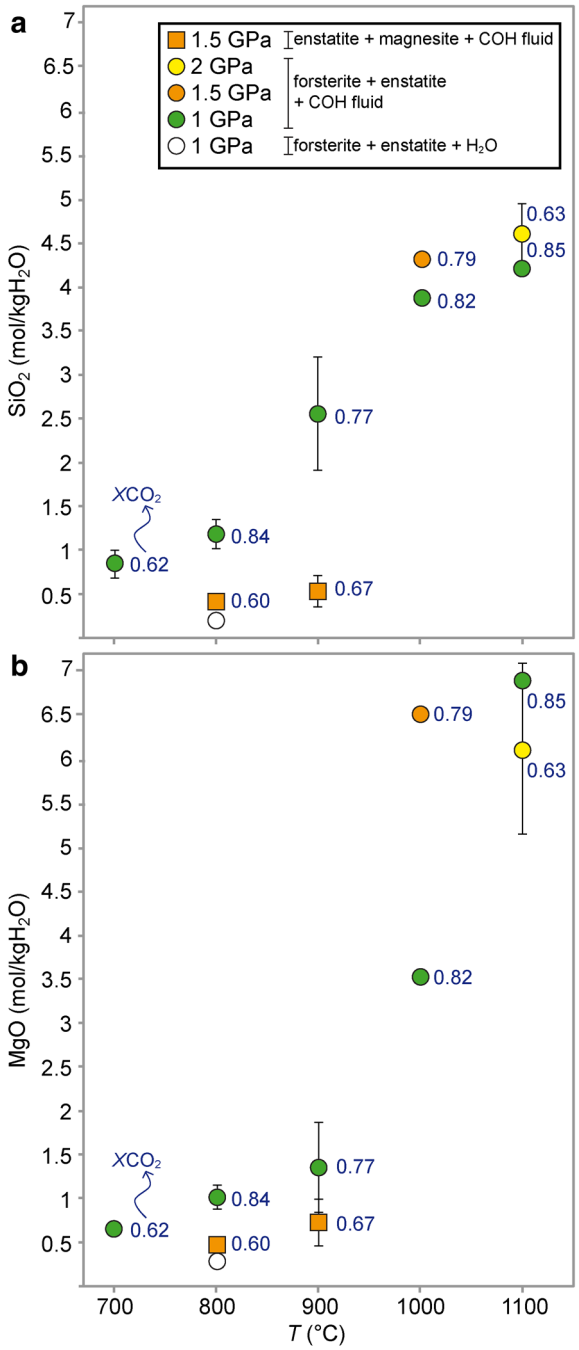

Fig. 5 Measured (by cryogenic LA-ICP-MS) silica and magnesia solubilities in the aqueous fraction of the COH fluid as a function of P and T expressed as mol SiO_2 per kg of water (**a**) and mol MgO per kg of water (**b**). Solute contents in the MSH system (white dots) are shown for comparison

however, we also have to consider that the pressure conditions are different (1.5 GPa for en + mgs; 1 GPa for fo + en) and the MgO could derive from either magnesite or enstatite, or from a combined effect.

Discussion

Comparison with previous solubility studies

In this experimental study, we provide for the first time solubility measurements of forsterite, enstatite and magnesite in a mixed H_2O–CO_2 fluid in equilibrium with graphite. To validate our approach, we also performed an experimental run in the system MgO–SiO_2–H_2O (MSH), to compare the results of our analytical technique with those obtained in previous studies on mineral solubility. Our experimental data relative to the dissolved SiO_2 in an aqueous fluid coexisting with forsterite and enstatite at 1 GPa and 800 °C ($mSiO_2 = 0.22$ mol/kg_{H2O}) is within error identical with the amount of SiO_2 determined by Newton and Manning (2002) ($mSiO_2 = 0.21$ mol/kg_{H2O}). Our experimental data fit quite well also with other literature data (Nakamura and Kushiro 1974; Manning and Boettcher 1994; Zhang and Frantz 2000; Newton and Manning 2002) on SiO_2 solubility in the same system (Fig. 6a, open symbols), demonstrating that different experimental strategies yield comparable results.

As far as the amount of MgO dissolved in an aqueous fluid with forsterite and enstatite is concerned, there are to

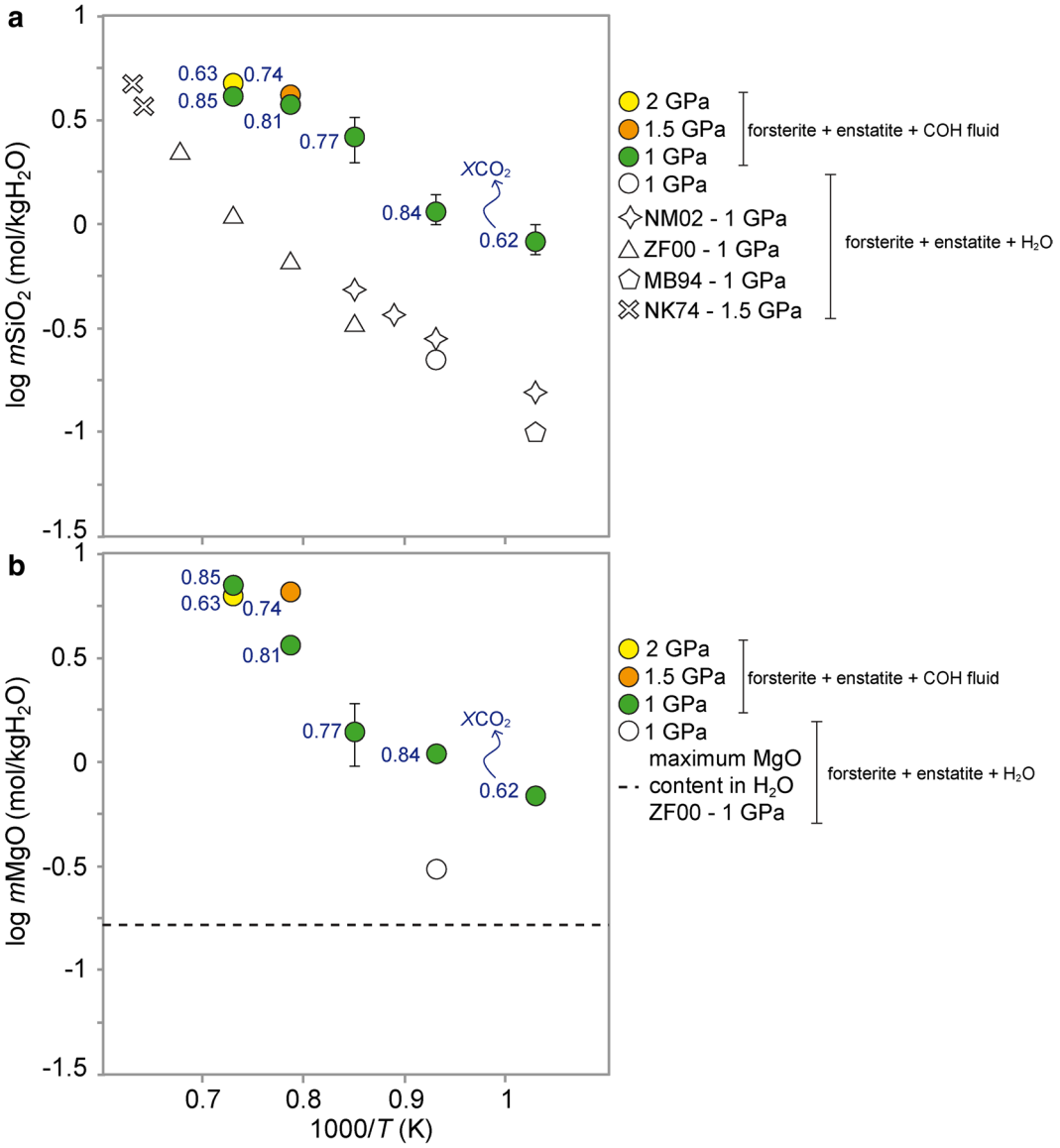

Fig. 6 Measured solute contents by cryogenic LA-ICP-MS in the aqueous fraction of the COH fluid as a function of inverse temperature at $P = 1$–2 GPa and $T = 700$–1100 °C, expressed as mol SiO_2 per kg of water (**a**) and mol MgO per kg of water (**b**). Solute content in the MSH system (white dots), and literature data are also shown for comparison. NM02: Newton and Manning (2002); ZF00: Zhang and Frantz (2000); MB94: Manning and Boettcher (1994); NK74: Nakamura and Kushiro (1974)

date no published experimental data available for the *P*–*T* conditions of 1 GPa and 800 °C investigated here. Extrapolation of MgO solubility derived from the dissolution of forsterite and enstatite in pure water from data obtained at $P = 1$–2 GPa and $T = 900$–1200 °C reported in Zhang and Frantz (2000) suggests a solubility below 0.17 mol/kg_{H2O} for our experimental conditions. Our measured fluid mMgO = 0.28 mol/kg_{H2O} (Fig. 6b) is higher. However, because our value represents the first experimental direct measurement at moderately high pressure of dissolved MgO in the MgO–SiO_2–H_2O system, this discrepancy cannot be evaluated further.

Dissolution of forsterite, magnesite and enstatite in COH fluids and comparisons with dissolution in H_2O

Compared with the solubility in the MgO–SiO_2–H_2O system, both the amounts of SiO_2 and MgO dissolved in the aqueous fraction of a COH fluid from forsterite + enstatite are higher (Fig. 6). This result suggests that in the MS + COH system, in contrast to what is observed for instance in the SiO_2–H_2O–CO_2 system (Newton and Manning 2000), the CO_2 component of the COH fluid does not act merely as an inert diluent, i.e., lowering the amount of solutes dissolved in the fluid. Instead, carbon dioxide seems to promote the dissolution of Mg-bearing silicates, favoring the formation of complexes involving Mg and C, as suggested by the higher MgO content in the aqueous fraction of COH fluid compared to the MgO dissolved in H_2O at the same experimental conditions ($P = 1$ GPa and $T = 800$ °C). As the amount of SiO_2 in the aqueous fraction of COH fluid is also higher compared to the dissolved SiO_2 in H_2O, our results indicate the formation of complexes potentially involving Mg, C and Si, in addition to the solutes generated by the effect of the aqueous component of the COH fluid (e.g., silica monomers and dimers as suggested by Newton and Manning 2002). The presence of Si–C complexes has not been previously detected in the system SiO_2–H_2O–CO_2, where the main dissolved species was thought to be a neutral dihydrate silica with one to three attached (solvated) H_2O molecules (Newton and Manning 2000). However, it should be noted that the cited experiments did not involve graphite.

There are two possible options to account for the increase in dissolved SiO_2 in the MS + COH system: (1) the generation of Mg–Si–C complexes, and (2) the production of a SiO_2 residue due to the formation of Mg–C solutes from forsterite and enstatite, which is highly soluble in H_2O (Manning 1994). In this experimental study, the dissolution process has been quantified in terms of absolute major elements solubilities in the fluid; therefore, information on the solutes speciation can only be gained indirectly, through thermodynamic modeling. However, the formation of SiO_2 and Mg–C solutes has been directly observed in the experimental runs where the solubility data were not retreived ($P > 2$ GPa and $T > 1100$ °C), as the diamond trap was no longer preserved. In these runs, the fluid was not completely ablated during LA-ICP-MS measurement; therefore, it was possible to characterize precipitates by backscattered electron (BSE) imaging of unpolished and polished samples. At 2.1 GPa and 1100 °C, precipitates appear as spheres of amorphous silica (Fig. 7a) and as vesiculated aggregate or acicular Mg–C solutes, probably hydrated (Fig. 7b). WDS analyses show detectable Cs quantity (up to 0.07 wt%), while for other solid phases Cs was below detection limit, confirming an origin as fluid quench precipitate. Moreover, we note that in this experimental run, only few diamonds were retrieved. We suggest that diamond dissolution could have occurred at the experimental conditions. Fedortchouk et al. (2007) at $P = 1$ GPa and $T = 1350$ °C observed that after 35 h, a diamond of 5 mm loses nearly 40 wt% of its initial weight at NNO oxygen fugacity conditions. Considering that the diamonds employed in our studies are significantly smaller (20 μm) while the experimental pressure is higher ($P = 2$–2.1 GPa), dissolution seems to be the process most plausible for the lack of diamonds, at least at the highest temperature conditions.

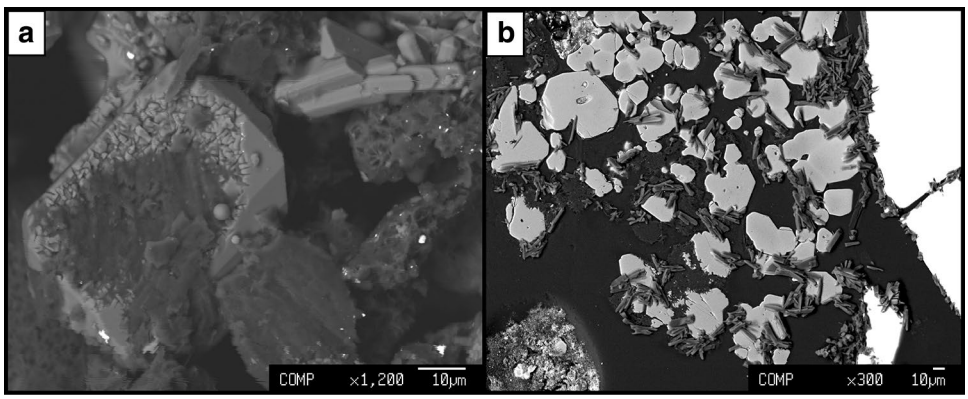

Fig. 7 Quench products from experiment at 2.1 GPa and 1100 °C. Amorphous silica precipitates on a corroded enstatite crystal (**a**), and acicular Mg–C precipitates with forsterite crystals (**b**)

At higher temperature ($P = 2$ GPa and $T = 1200$ °C) forsterite, diamond and graphite were completely dissolved in a silica-rich vesiculated glass with few enstatite crystals dispersed (see Fig. 4b). The observed texture is extremely similar to an experimental run performed by Cruz and Manning (2015) in the SiO_2–H_2O–NaCl system at 1.5 GPa and 1100 °C. In this case, the authors suggested that a similar feature indicates the presence of two distinct fluids, one hydrous Si-rich fluid and the other saline and relatively Si-poor. In our experimental runs, the relatively Si-poor fluid could be constituted by Mg–C complexes, as shown in Fig. 7b ($P = 2.1$ GPa and $T = 1100$ °C). However, it remains unclear why in the experimental run at 2 GPa and 1200 °C the Mg-bearing fluid was not identified. Moreover, the presence of a miscibility gap seems unlikely in a NaCl-free system and could result simply from the quench process.

In Fig. 8, the solubilities of silica and magnesia are plotted versus the XCO_2 of the coexisting COH fluid. In both cases, we observe an increase with temperature and XCO_2. However, the behavior of SiO_2 and MgO is different when it comes to increasing pressure: while the SiO_2 content tends to increase (Fig. 8a), the dissolved MgO shows higher values at lower pressure and high temperature conditions ($P = 1$ GPa; $T = 1100$ °C), where the COH fluid is mainly composed by CO_2 ($XCO_2 = 0.85$) (Fig. 8b). We suggest that at high temperature conditions, CO_2 favors the formation of Mg–C complexes, while H_2O, present in significantly minor quantity, appear to dissolve less SiO_2. With increasing pressure, the XCO_2 lowers; consequently less MgO is dissolved in the fluid, while the aqueous component becomes more effective in dissolving the SiO_2 residue.

The amount of solutes derived from the dissolution of the assemblage magnesite + enstatite in a COH fluid can be compared to the experimental data from Caciagli and Manning (2003) relative to calcite dissolution in H_2O. The dissolved cations in this experimental study are Mg and Si instead of Ca, and the volatiles present in the initial fluid are H_2O and CO_2 instead of pure H_2O. Solute amounts for Mg and Ca are similar and in agreement with literature data (Fig. 9), suggesting similar solubilities for $CaCO_3$ and $MgCO_3$ at the *PT* conditions investigated here, irrespective of the more complex chemistry of our system. Thermodynamic models indicate that pure magnesite is slightly soluble in H_2O at 10 GPa (Pan et al. 2013) and has a lower solubility compared to calcite over a significant pressure range (1–10 GPa). This comparison shows that either (1) the addition of CO_2 to an aqueous fluid enhances magnesite dissolution compared to H_2O, or (2) that solvation of Mg in our experimental system involves Mg–Si species, or both. Concerning possibility (1), we observe that our experimental amount of SiO_2 dissolved from enstatite is quite similar to that in H_2O (0.41 mol/kg_{H2O} in COH fluid at 1.5 GPa and 800 °C versus 0.42 mol/kg_{H2O} at 1 GPa and

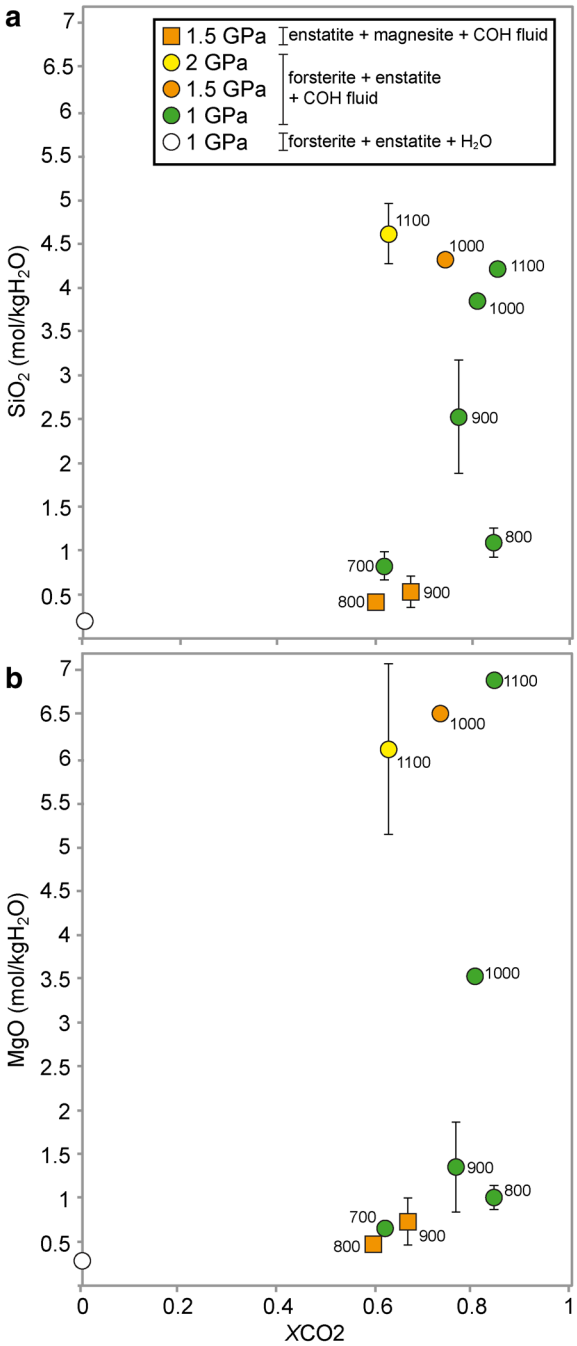

Fig. 8 Measured solute contents by cryogenic LA-ICP-MS in the aqueous fraction of COH fluid, plotted versus the XCO_2 of the coexisting COH fluid at $P = 1$–2 GPa and $T = 700$–1100 °C, expressed as mol SiO_2 per kg of water (**a**) and mol MgO per kg of water (**b**)

850 °C, Newton and Manning 2002). Our SiO_2 solubilities at 1.5 GPa and 900 °C (0.53 mol/kg_{H2O}) are similar to those obtained for pure water coexisting with enstatite + forsterite at 1.4 GPa and 900 °C (0.51–0.52 mol/kg_{H2O}; Newton and Manning 2002). SiO_2 dissolution thus seems to

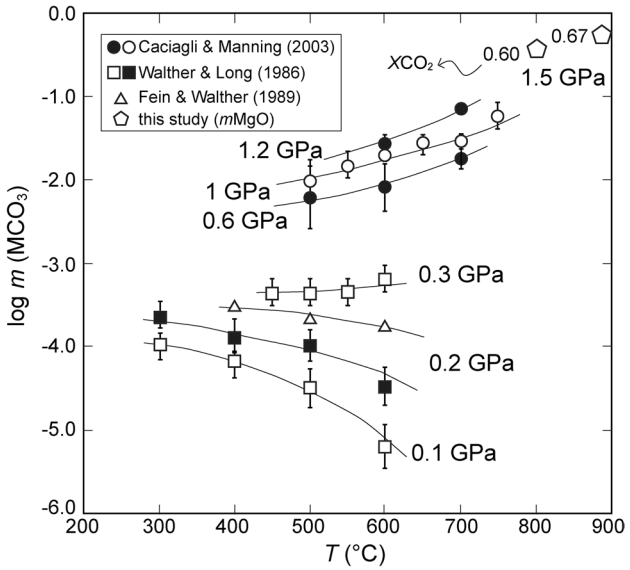

Fig. 9 Solubility of MCO_3 (M=Ca or Mg) in H_2O. $CaCO_3$ data: Caciagli and Manning (2003), Walther and Long (1986) and Fein and Walther (1989); $MgCO_3 + MgSiO_3$ data: this study. Our experimental results on magnesite + enstatite solubility in COH fluid at 1.5 GPa are expressed as *m*MgO (mol/kg_{H2O})

be governed by the H_2O component, and no positive or negative effect caused by CO_2 addition to the fluid can be discerned. For what concerned the MgO content, due to the lack of experimental measures of MgO from enstatite and magnesite dissolution in H_2O, we cannot evaluate if the measured MgO in the aqueous fraction of the COH fluid derives from the dissolution of either enstatite or magnesite, or from a combined effect.

Theoretical solute speciation modeling

To characterize the possible aqueous species relevant to our experimental system, we employed a thermodynamic model that, in addition to neutral COH species, also takes into account Mg and Si-bearing dissolved species. We performed calculations using the aqueous speciation-solubility code EQ3 (Wolery 1992) adapted to include equilibrium constants calculated with the Deep Earth Water (DEW) model (Facq et al. 2014; Sverjensky et al. 2014). We focused on the solubility measurements at 800 °C and 1.0 GPa, as results were available for the solubility of MgO and SiO_2 in the MSH system as well as the MS + COH system. The two sets of MgO and SiO_2 solubility data enabled characterization of a Mg–OH complex and a Mg–Si–C complex.

For the MSH system, silica concentrations predicted using the silica monomer and dimer in the DEW model agreed, as expected, with the experimentally measured values. However, matching the experimental Mg concentration required a $Mg(OH)_2$ complex in addition to the predicted value for $Mg(OH)^+$. Trial and error regressions of the experimental data for the MSH and the MS + COH systems indicated that $Mg(OH)^+$ could not account for the measured Mg concentrations in both systems. Instead, the data for the MSH system were used to retrieve the equilibrium constant for the second $Mg(OH)_2$ complex given by the equilibrium:

$$Mg(OH)_2 + 2H^+ = Mg^{2+} + 2H_2O, \quad (11)$$

as in Table 3.

In the system MS + COH, the model Mg-solubilities using the new Mg–OH complexes were still too low, indicating the likely need for additional Mg-bearing complex. Furthermore, the predicted Si-solubility based solely on

Table 3 Calculated model values of the solubility of forsterite + enstatite in water and forsterite + enstatite in COH fluid (Calc.) at fH_2 values calculated from thermodynamic modeling (see Table 1) compared with the experimentally measured values (Exp.)

	Run	*P* (GPa)	*T* (°C)	log fH_2	pH	$mSiO_2$	*m*MgO	$Mg(OH)_2$[a]	MgSiC[b]	$Si(OH)_4$[c]	Si-dimer[d]
Forsterite + Enstatite + Graphite + COH fluid											
Exp	29	1.0	800			1.24 (0.19)	1.08 (0.10)				
Calc		1.0	800	1.78	3.73	1.15	1.22	0.11	1.11	0.039	0.00028
Forsterite + Enstatite + H_2O											
Exp	22	1.0	800			0.22 (0.06)	0.28 (0.04)				
Calc		1.0	800	1.78	5.57	0.29	0.26	0.26	–	0.21	0.035

Solubilities and aqueous species concentrations are expressed as mol/kg_{H2O}. Experimental uncertainties in parentheses as in Table 2

[a]$Mg(OH)_2$ stands for the Mg-complex in the equilibrium $Mg(OH)_2 + 2H^+ = Mg^{2+} + 2H_2O$ for which the logK = 3.9 at 800 °C and 1.0 GPa was obtained by fitting the experimental data for Forsterite + Enstatite + H_2O in the table

[b]MgSiC stands for the Mg-complex in the equilibrium $Mg[OSi(OH_3)][CH_3CH_2COO] + H^+ = Mg^{2+} + SiO_{2,aq} + CH_3CH_2COO^- + H_2O$ for which the logK = −7.0 at 800 °C and 1.0 GPa was obtained by fitting the experimental data for Forsterite + Enstatite + Graphite + COH fluid in the table

[c]$Si(OH)_{4,aq}$ stands for the silica monomer molality

[d]Si-dimer stands for the silica dimer in the equilibrium $Si(OH)_3OSi(OH)_3 + H_2O = 2Si(OH)_4$ for which the equilibrium constant logK = 0.1083 at 800 °C and 1.0 GPa (Sverjensky et al. 2014)

the monomer and dimer was also way too low because it remained the same as for the C-free system (Table 3). Trial and error regressions using various species such as $MgHCO_3^+$, $MgCO_3$, $MgHSiO_3^+$, and $MgSiO_3$ failed to adequately describe the experimental data for the MS + COH system given what was already known about the stabilities of these complexes. Instead, the data for the MS + COH system was used to retrieve the equilibrium constant for a complex involving Mg, Si, and C according to the equilibrium:

$$Mg\left[OSi(OH_3)\right]\left[CH_3CH_2COO\right] + H^+ = Mg^{2+} + SiO_{2,aq} + CH_3CH_2COO^- + H_2O, \quad (12)$$

as in Table 3. This complex, which involves carbon, results in the solubility of MgO and SiO_2 fO_2 dependent. Propionate involves reduced C. Therefore, calculated solubilities involving Eq. (12) increase at lower fO_2 values and decrease at higher fO_2 values. Equation (12) is only relevant for reducing systems. It should not be significant at all in COH fluids from all previous studies of Mg-silicate solubilities or stabilities that have focused on oxidizing conditions without graphite. Consequently, Eq. (12) provides an explanation for the distinctive enhanced solubilities of Mg and Si measured in the present study, which does involve graphite, and, presumably, aqueous species involving reduced carbon. Volatile reduced C-species have in fact been detected in chemical analyses of the volatiles present in the MS + COH system with graphite (Tumiati et al. 2017), as well as implied by model calculations of the COH fluid volatile compositions (Table 1).

A more complete analysis of the potential importance of Eq. (12) over a wide range of temperatures and pressures is hampered by the lack of experimental Mg-solubility data in the MSH system, which is needed for quantification of Eq. (11). Consequently, a full characterization of the standard partial molal properties of the Mg–Si–C-complex must await the development of several estimation schemes for predicting the properties of the Mg–OH complex in Eq. (11). This will be the subject of a future study.

Forsterite carbonation reaction

Although the experiments performed were aimed to measure solutes composition and were not reversed, we reported in Fig. 2 the forsterite carbonation curve in presence of a COH fluid (Reaction 7). The reaction shows a weak pressure dependency and occurs at higher pressure compared to the one determined by Koziol and Newton (1998) in the $MgO–SiO_2–CO_2$ system. The shift toward higher pressures, predicted by the calculated reaction through thermodynamic modeling, is caused by the presence of H_2O in the investigated experimental system (Eggler et al. 1979). With increasing temperatures the forsterite + COH fluid reaction approaches the curve proposed by Koziol and Newton (1998) as the composition of the COH fluid becomes more CO_2 rich.

Implications for metasomatic processes

Several authors investigated the MSH system as a simplified model for melting and solubility in hydrated peridotites (e.g., Kushiro 1969; Ryabchikov et al. 1982; Inoue 1994; Luth 1995; Zhang and Frantz 2000; Stalder et al. 2001; Mibe et al. 2002; Hack et al. 2007). Available experimental data on mineral solubility in this system indicates that at low-pressure conditions (< 3 GPa) the amount of dissolved SiO_2 in the aqueous fluid is significantly higher compared to MgO (e.g., Zhang and Frantz 2000; Newton and Manning 2002). At these conditions, an aqueous fluid, migrating upward through the upper mantle, dissolves up to the 20 wt% of silica, leaving a SiO_2-depleted mantle and a relatively SiO_2-enriched crust (Nakamura and Kushiro 1974). This process results in the formation of enstatite relative to forsterite, as the MgO/SiO_2 ratio of the fluid is expected to be significantly lower than unity. However, this ratio derives from experimental data limited to SiO_2, as no direct measures of MgO solubility in aqueous fluid are available at low-pressure conditions. Our experimental study presents for the first time the amount of both SiO_2 and MgO dissolved in an aqueous fluid in equilibrium with forsterite and enstatite (MSH system), and consequently provides the first experimentally based MgO/SiO_2 ratio of the fluid at low-pressure conditions. At 1 GPa and 800 °C, the aqueous fluid shows a higher MgO/SiO_2 ratio (= 1.27) than previously estimated in literature (e.g., Kawamoto et al. 2004a).

In Fig. 10 a *T*–*X* isobaric pseudosection is presented to show the effect of variable MgO/SiO_2 ratios in a fluid reacting with forsterite. Assuming a complete reaction between 25 mol% of fluid and 75 mol% of forsterite, fluids with MgO/SiO_2 ratios < 2 will modify the system bulk compositions, so that enstatite may form. In the MSH system, the amount of enstatite produced by an aqueous fluid at 1 GPa and 800 °C, is approximately + 9 mol% (open symbol in Fig. 10) and the calculated amount of fluid required to complete the reaction is 602 g of water for one mole of forsterite (g_{H2O}/mol forsterite). In the MS + COH system, the MgO/SiO_2 ratio of the fluid is lower compared to the MSH system (filled symbols in Fig. 10) and tends to increase with temperature. At 1 GPa and 800 °C, the amount of produced enstatite is slightly higher (+ 14 mol%), however the fluid required for the reaction to occur is significantly lower compared to the MSH system (129 g_{H2O}/mol forsterite versus 602 g_{H2O}/forsterite). With increasing temperatures the amount of orthopyroxene decreases to < 5 mol% at 1 GPa and 1100 °C, with 27 g_{H2O}/mol forsterite employed in the reaction forsterite + fluid (MgO/SiO_2 = 1.64). Therefore, in

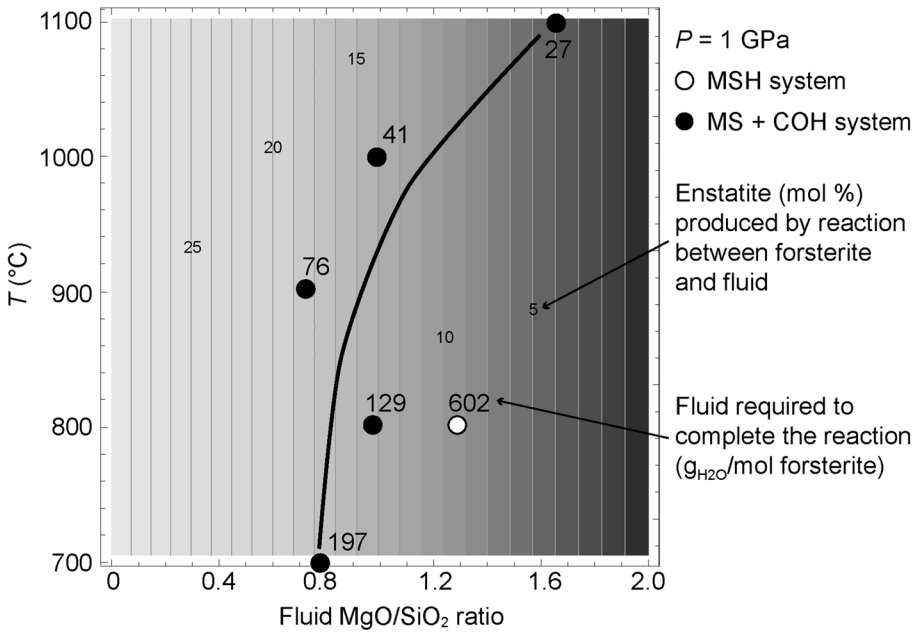

Fig. 10 Thermodynamic modeling of forsterite reacting with a fluid with variable MgO/SiO_2 ratio. *T*–*X* isobaric section calculated at fixed *P* = 1 GPa where *X* = 0 stands for 1 mol forsterite + 0.3 mol SiO_2 (fluid MgO/SiO_2 = 0) and *X* = 2 represents 1 mol forsterite + 0.2 mol MgO + 0.1 mol SiO_2 (MgO/SiO_2 = 2). The amount of fluid required to complete the reaction expressed as g_{H2O}/mol forsterite is also reported. The trend of MgO/SiO_2 ratios was drawn by eye

the MS + COH system, lower quantities of fluid will metasomatize the forsterite compared to the MSH system, where significant amounts of water are required to complete the reaction forsterite + fluid.

In a mantle wedge flushed by H_2O and CO_2 in the presence of graphite (Galvez et al. 2013), where subsolidus conditions prevail, solute-rich fluids can deeply affect the surrounding peridotite, leading to the formation of enstatite-enriched levels. This process appears to be favored by the presence of CO_2 compared to a system where the only volatile species is H_2O.

Orthopyroxenites formation in the mantle wedge has been documented in literature as a consequence of slab-derived SiO_2-rich aqueous fluids (e.g., Malaspina et al. 2006, 2017; Campione et al. 2017). Our results suggest that the occurrence of orthopyroxene-enriched layers could also be linked to the effect of Mg- and Si-rich COH fluids, which are able to transport higher amounts of solute compared to an aqueous fluid. Metasomatic processes driven by solute-rich COH fluid could represent a further mechanism to account for the Si-enrichment and the consequent formation of orthopyroxenites in the upper mantle, in addition to processes such as interaction with crustal rocks and/or Si-rich melts.

Conclusions

In this experimental work, we present the first measurements of dissolved SiO_2 and MgO in graphite-saturated COH fluids from two different assemblages, forsterite + enstatite and magnesite + enstatite. We employed the cryogenic LA-ICP-MS technique on double-capsule assemblages to quantify SiO_2 and MgO solubility in the aqueous fraction of COH fluids buffered at NNO oxygen fugacity conditions. The presence of CO_2 increases the solubility of forsterite and enstatite compared to systems containing only H_2O as volatile component. Moreover, magnesite solubility in a COH fluid is similar to that of calcite in pure H_2O and surprisingly lower compared to forsterite + enstatite solubility in COH fluids.

Our results indicate that in a Mg-bearing system CO_2 does not act merely as an inert diluent, by lowering the solubility of solid phases. On the contrary, CO_2 favors the formation of Mg–Si–C complexes, leading to a graphite-saturated COH fluid containing significant amounts of dissolved reduced carbon species. The molality of this fluid increases greatly with temperature and quintuplicates with respect to C-free aqueous fluids. In the mantle wedge, the amount of fluid necessary to metasomatize the surrounding peridotite decreases in the presence of carbon with increasing temperatures, leading to the formation of orthopyroxene-rich levels. Recently, it has been demonstrated that silicate dissolution controls the compositions of COH fluids in equilibrium with graphite (Tumiati et al. 2017), by increasing their CO_2 content (+ 30%) compared to silicate-free systems. Independently from the occurrence of carbonates, dissolution of silicates can boost the dissolution of graphite in the subduction mélange in the form of volatile CO_2 dissolved in COH fluids. Solute-rich, graphite-saturated H_2O–CO_2 fluid could therefore represent an effective way to mobilize C-bearing species to shallowest levels in the upper mantle, along with other processes such as diapirism of slab rocks (Marschall and Schumacher 2012; Tumiati et al. 2013) and carbonatitic melt generation (Poli 2015).

From an analytical point of view, the cryogenic LA-ICP-MS technique, coupled with other techniques to characterize the volatile speciation of the fluid (e.g., Tiraboschi et al. 2016) represents a significant improvement towards a comprehensive characterization of high-pressure fluids, in terms of volatile speciation and dissolved solute species.

Acknowledgements The authors are indebted to A. Risplendente for the assistance with scanning electron microscope and electron microprobe. Editorial handling by M.W. Schmidt, O. Müntener, and reviews from two anonymous reviewers significantly improved the manuscript. Funding was provided by the Italian Ministry of Education, University and Research (MIUR) program PRIN2012R33ECR. C.T., S.T., D.S. and S.P. acknowledge supports from the Deep Carbon Observatory (DCO).

References

Aerts M, Hack AC, Reusser E, Ulmer P (2010) Assessment of the diamond-trap method for studying high-pressure fluids and melts and an improved freezing stage design for laser ablation ICP-MS analysis. Am Mineral 95:1523–1526

Anderson GM, Burnham CW (1965) The solubility of quartz in supercritical water. Am J Sci 263:494–511

Aranovich LY, Newton RC (1999) Experimental determination of CO_2–H_2O activity-composition relations at 600–1000 °C and 6–14 kbar by reversed decarbonation and dehydration reactions. Am Mineral 84:1319–1332

Baker MB, Stolper EM (1994) Determining the composition of high-pressure mantle melts using diamond aggregates. Geochim Cosmochim Acta 58:2811–2827. https://doi.org/10.1016/0016-7037(94)90116-3

Caciagli NC, Manning CE (2003) The solubility of calcite in water at 6–16 kbar and 500–800 °C. Contrib to Mineral Petrol 146:275–285. https://doi.org/10.1007/s00410-003-0501-y

Campione M, Tumiati S, Malaspina N (2017) Primary spinel + chlorite inclusions in mantle garnet formed at ultrahigh-pressure. Geochem Persp Let 4:19–23. https://doi.org/10.7185/geochemlet.1730

Connolly JAD (1990) Multivariable phase-diagrams—an algorithm based on generalized thermodynamics. Am J Sci 290:666–718

Connolly JAD, Cesare B (1993) C–O–H–S fluid composition and oxygen fugacity in graphitic metapelites. J Metamorph Geol 11:379–388

Cruz MF, Manning CE (2015) Experimental determination of quartz solubility and melting in the system SiO_2–H_2O–NaCl at 15–20 kbar and 900–1100 °C: implications for silica polymerization and the formation of supercritical fluids. Contrib to Mineral Petrol 170:35. https://doi.org/10.1007/s00410-015-1187-7

Dolejs D, Manning CE (2010) Thermodynamic model for mineral solubility in aqueous fluids: theory, calibration and application to model fluid-flow systems. Geofluids 10:20–40. https://doi.org/10.1111/j.1468-8123.2010.00282.x

Eggler DH, Kushiro I, Holloway JR (1979) Free energies of decarbonation reactions at mantle pressures; I, Stability of the assemblage forsterite-enstatite-magnesite in the system MgO–SiO_2–CO_2–H_2O to 60 kbar. Am Mineral 64:288–293

Eugster HP, Skippen GB (1967) Igneous and metamorphic reactions involving gas equilibria. Res Geochem 2:492–520

Facq S, Daniel I, Montagnac G, Cardon H, Sverjensky D (2014) In situ Raman study and thermodynamic model of aqueous carbonate speciation in equilibrium with aragonite under subduction zone conditions. Geochim Cosmochim Acta 132:375–390. https://doi.org/10.1016/j.gca.2014.01.030

Fedortchouk Y, Canil D, Semenets E (2007) Mechanisms of diamond oxidation and their bearing on the fluid composition in kimberlite magmas. Am Mineral 92:1200–1212. https://doi.org/10.2138/am.2007.2416

Fein JB, Walther JV (1989) Calcite solubility and speciation in supercritical NaCl–HCl aqueous fluids. Contrib to Mineral Petrol 103:317–324. https://doi.org/10.1007/BF00402918

Galvez ME, Beyssac O, Martinez I, Benzerara K, Chaduteau C, Malvoisin B, Malavieille J (2013) Graphite formation by carbonate reduction during subduction. Nat Geosci 6:473–477. https://doi.org/10.1038/ngeo1827

Guillong M, Meier DL, Allan MM, Heinrich CA, Yardley BW (2008) Appendix A6: SILLS: a MATLAB-based program for the reduction of laser ablation ICP-MS data of homogeneous materials and inclusions. Mineral Assoc Canada Short Course Ser 40:328–333

Hack AC, Thompson AB, Aerts M (2007) Phase relations involving hydrous silicate melts, aqueous fluids, and minerals. Rev Mineral Geochem 65:129–185. https://doi.org/10.2138/rmg.2007.65.5

Holland TJB, Powell R (1998) An internally consistent thermodynamic data set for phases of petrological interest. J Metamorph Geol 16:309–343. https://doi.org/10.1111/j.1525-1314.1998.00140.x

Inoue T (1994) Effect of water on melting phase relations and melt composition in the system Mg_2SiO_4–$MgSiO_3$–H_2O up to 15 GPa. Phys Earth Planet Int 85:237–263

Kawamoto T, Matsukage KN, Mibe K, Isshiki M, Nishimura K, Ishimatsu N, Ono S (2004a) Mg/Si ratios of aqueous fluids coexisting with forsterite and enstatite based on the phase relations in the Mg_2SiO_4–SiO_2–H_2O system. Am Mineral 89:1433–1437

Kawamoto T, Ochiai S, Kagi H (2004b) Changes in the structure of water deduced from the pressure dependence of the Raman OH frequency. J Chem Phys 120:5867–5870. https://doi.org/10.1063/1.1689639

Kessel R, Ulmer P, Pettke T, Schmidt MW, Thompson AB (2004) A novel approach to determine high-pressure high-temperature fluid and melt compositions using diamond-trap experiments. Am Mineral 89:1078–1086

Kessel R, Schmidt MW, Ulmer P, Pettke T (2005a) Trace element signature of subduction-zone fluids, melts and supercritical liquids at 120–180 km depth. Nature 437:724–727. https://doi.org/10.1038/nature03971

Kessel R, Ulmer P, Pettke T, Schmidt MW, Thompson AB (2005b) The water-basalt system at 4 to 6 GPa: phase relations and second critical endpoint in a K-free eclogite at 700 to 1400 °C. Earth Planet Sci Lett 237:873–892. https://doi.org/10.1016/j.epsl.2005.06.018

Koziol AM, Newton RC (1998) Experimental determination of the reaction: magnesite + enstatite = forsterite + CO_2 in the ranges 6–25 kbar and 700–1100 °C. Am Mineral 83:213–219

Kushiro I (1969) System forsterite-diopside-silica with and without water at high pressures. Am J Sci 267A:269–294

Luth RW (1989) Natural versus experimental control of oxidation state : effects on the composition and speciation of C–O–H fluids. Am Mineral 74:50–57

Luth RW (1995) Is phase A relevant to the Earth's mantle? Geochim Cosmochim Acta 59:679–682. https://doi.org/10.1016/0016-7037(95)00319-U

Malaspina N, Hermann J, Scambelluri M, Compagnoni R (2006) Polyphase inclusions in garnet–orthopyroxenite (Dabie Shan, China) as monitors for metasomatism and fluid-related trace element transfer in subduction zone peridotite. Earth Planet Sci Lett 249:173–187. https://doi.org/10.1016/j.epsl.2006.07.017

Malaspina N, Langenhorst F, Tumiati S, Campione M, Frezzotti ML, Poli S (2017) The redox budget of crust-derived fluid phases at the slab-mantle interface. Geochim Cosmochim Acta 209:70–84. https://doi.org/10.1016/j.gca.2017.04.004

Manning CE (1994) The solubility of quartz in H_2O in the lower crust and upper mantle. Geochim Cosmochim Acta 58:4831–4839. https://doi.org/10.1016/0016-7037(94)90214-3

Manning CE, Boettcher SL (1994) Rapid-quench hydrothermal experiments at mantle pressures and temperatures. Am Mineral 79:1153–1158

Marschall HR, Schumacher JC (2012) Arc magmas sourced from mélange diapirs in subduction zones. Nat Geosci 5:862–867. https://doi.org/10.1038/ngeo1634

Melekhova E, Schmidt MW, Ulmer P, Pettke T (2007) The composition of liquids coexisting with dense hydrous magnesium silicates at 11–13.5 GPa and the endpoints of the solidi in the $MgO–SiO_2–H_2O$ system. Geochim Cosmochim Acta 71:3348–3360. https://doi.org/10.1016/j.gca.2007.03.034

Mibe K, Fujii T, Yasuda A (2002) Composition of aqueous fluid coexisting with mantle minerals at high pressure and its bearing on the differentiation of the Earth's mantle. Geochim Cosmochim Acta 66:2273–2285. https://doi.org/10.1016/S0016-7037(02)00856-6

Nakamura Y, Kushiro I (1974) Composition of the gas phase in $Mg_2SiO_4–SiO_2–H_2O$ at 15 kbar. Carnegie Inst Washingt Yearb 73:255–258

Newton RC, Manning CE (2000) Quartz solubility in $H_2O–NaCl$ and $H_2O–CO_2$ solutions at deep crust-upper mantle pressures and temperatures: 2–15 kbar and 500–900 °C. Geochim Cosmochim Acta 64:2993–3005. https://doi.org/10.1016/S0016-7037(00)00402-6

Newton RC, Manning CE (2002) Solubility of enstatite + forsterite in H_2O at deep crust/upper mantle conditions: 4 to 15 kbar and 700 to 900 °C. Geochim Cosmochim Acta 66:4165–4176. https://doi.org/10.1016/S0016-7037(02)00998-5

Newton RC, Manning CE (2009) Hydration state and activity of aqueous silica in $H_2O–CO_2$ fluids at high pressure and temperature. Am Mineral 94:1287–1290. https://doi.org/10.2138/am.2009.3287

Pan D, Galli G (2016) The fate of carbon dioxide in water-rich fluids at extreme conditions. Sci Adv. https://doi.org/10.1126/sciadv.1601278

Pan D, Spanu L, Harrison B, Sverjensky DA, Galli G (2013) Dielectric properties of water under extreme conditions and transport of carbonates in the deep Earth. Proc Natl Acad Sci USA 110:6646–6650. https://doi.org/10.1073/pnas.1221581110

Pettke T, Oberli F, Audétat A, Guillong M, Simon AC, Hanley JJ, Klemm LM (2012) Recent developments in element concentration and isotope ratio analysis of individual fluid inclusions by laser ablation single and multiple collector ICP-MS. Ore Geol Rev 44:10–38. https://doi.org/10.1016/j.oregeorev.2011.11.001

Poli S (2015) Carbon mobilized at shallow depths in subduction zones by carbonatitic liquids. Nat Geosci 8:633–636. https://doi.org/10.1038/ngeo2464

Ryabchikov ID, Schreyer W, Abraham K (1982) Compositions of aqueous fluids in equilibrium with pyroxenes and olivines at mantle pressures and temperatures. Contrib Miner Pet 79:80–84. https://doi.org/10.1007/BF00376964

Ryabchikov ID, Brey G, Kogarko LN, Bulatov VK (1989) Partial melting of carbonatised peridotite at 50 kbar. Geochem Int 26:1–7

Sanchez-Valle C, Martinez I, Daniel I, Philippot P, Bohic S, Simionovici A (2003) Dissolution of strontianite at high P-T conditions: an in-situ synchrotron X-ray fluorescence study. Am Mineral 88:978–985

Schmidt MW, Ulmer P (2004) A rocking multianvil: elimination of chemical segregation in fluid-saturated high-pressure experiments. Geochim Cosmochim Acta 68:1889–1899. https://doi.org/10.1016/j.gca.2003.10.031

Schneider ME, Eggler DH (1986) Fluids in equilibrium with peridotite minerals: Implications for mantle metasomatism. Geochim Cosmochim Acta 50:711–724. https://doi.org/10.1016/0016-7037(86)90347-9

Shmulovich KI, Graham CM, Yardley BWD (2001) Quartz, albite and diopside solubilities in $H_2O–NaCl$ and $H_2O–CO_2$ fluids at 0.5–0.9 GPa. Contrib Miner Pet 141:95–108. https://doi.org/10.1007/s004100000224

Shmulovich KI, Yardley BWD, Graham CM (2006) Solubility of quartz in crustal fluids: experiments and general equations for salt solutions and $H_2O–CO_2$ mixtures at 400–800 °C and 0.1–0.9 GPa. Geofluids 6:154–167. https://doi.org/10.1111/j.1468-8123.2006.00140.x

Stalder R, Ulmer P, Thompson AB, Günther D (2001) High pressure fluids in the system $MgO–SiO_2–H_2O$ under upper mantle conditions. Contrib Miner Pet 140:607–618. https://doi.org/10.1007/s004100000212

Sverjensky DA, Harrison B, Azzolini D (2014) Water in the deep Earth: The dielectric constant and the solubilities of quartz and corundum to 60 kb and 1200 °C. Geochim Cosmochim Acta 129:125–145. https://doi.org/10.1016/j.gca.2013.12.019

Tiraboschi C, Tumiati S, Recchia S, Miozzi F, Poli S (2016) Quantitative analysis of COH fluids synthesized at HP–HT conditions: an optimized methodology to measure volatiles in experimental capsules. Geofluids 16:841–855. https://doi.org/10.1111/gfl.12191

Tumiati S, Fumagalli P, Tiraboschi C, Poli S (2013) An experimental study on COH-bearing peridotite up to 3.2 GPa and implications for crust-mantle recycling. J Petrol 54:453–479

Tumiati S, Tiraboschi C, Sverjensky D, Pettke T, Recchia S, Ulmer P, Miozzi F, Poli S (2017) Silicate dissolution boosts the CO_2 concentrations in subduction fluids. Nat Commun 8:616. https://doi.org/10.1038/s41467-017-00562-z

Walther JV, Long MI (1986) Experimental determination of calcite solubilities in supercritical H_2O. Int Symp Water-Rock Interact 5:609–611

Walther JV, Orville PM (1983) The extraction-quench technique for determination of the thermodynamic properties of solute complexes: application to quartz solubility in fluid mixtures. Am Mineral 68:731–741

Wolery TJ (1992) EQ3NR, A computer program for geochemical aqueous speciation-solubility calculations: theoretical manual, user's guide and related documentation (version 7.0)

Zhang C, Duan Z (2009) A model for C–O–H fluid in the Earth's mantle. Geochim Cosmochim Acta 73:2089–2102. https://doi.org/10.1016/j.gca.2009.01.021

Zhang C, Duan Z (2010) GFluid: An Excel spreadsheet for investigating C–O–H fluid composition under high temperatures and pressures. Comput Geosci 36:569–572. https://doi.org/10.1016/j.cageo.2009.05.008

Zhang YG, Frantz JD (2000) Enstatite-forsterite-water equilibria at elevated temperatures and pressures. Am Mineral 85:918–925